

Supporting Information

Angular-Resolved Rabi Oscillations of Orthorhombic Spins in a Co(II) Molecular Qubit

Yi-Qiu Liao,^a You-Chao Liu,^a Yi-Han Wang,^b Peng-Xiang Fu,^b Yi Xie,^a Song Gao,^{a,b,c}
Ye-Xin Wang,^{*d} Zheng Liu^{*c} and Shang-Da Jiang^{*a}

a. Spin-X Institute, School of Chemistry and Chemical Engineering, South China University of Technology, Guangzhou, 511442, China. E-mail: jiangsd@scut.edu.cn

b. Beijing National Laboratory of Molecular Science, Beijing Key Laboratory of Magnetoelectric Materials and Devices, College of Chemistry and Molecular Engineering, Peking University, Beijing (China).

c. Key Laboratory of Bioinorganic and Synthetic Chemistry of Ministry of Education, LIFM, School of Chemistry, IGCME, Sun Yat-Sen University, Guangzhou 510275, China. E-mail: liuzh363@mail.sysu.edu.cn

d. Quantum Science Centre of Guangdong-Hong Kong-Macao Greater Bay Area, Shenzhen, 518045, China. E-mail: wanyexin@quantumsc.cn

List of Supporting Information

SI 1 Supplementary Figures (Fig), Tables and Equations (Eq)

Table S1. Crystallographic data

Fig.S1. The result of face indexing showing on a physical crystal

Fig.S2. Powder X-ray diffraction

Fig.S3. Relative position between crystal frame and tensor frames

Fig.S4. T_1 and T_m curves at 5 K in the g_z direction

Fig.S5. Temperature dependence of T_1 at 3907 G

Table S2. T_1 and T_m data at 5 K in the g_z direction

Table S3. T_1 data at different temperatures at 3907 G

Fig.S6. Rabi oscillations measured at 5 K when $B_0 \parallel \mathbf{b}, B_1 \parallel \mathbf{a}$

Fig.S7. EDFS of the crystal with TEMPO internal standard

Eq.S1. Calculation formulas of internal standard method

Fig.S8. Rabi oscillation experiments when $B_1 \parallel g_z, g_x, g_y$

Fig.S9. Anisotropic Rabi oscillation experiments with internal standard

Fig.S10. Calibration of experimental rotation angle α

Fig.S11. T_1 and T_m curves at 5 K in the g_y direction

SI 2 Theoretical analysis of anisotropic Rabi oscillation (I)

SI 3 Theoretical analysis of anisotropic Rabi oscillation (II)

SI 1 Supplementary Figures (Fig), Tables and Equations (Eq)

Table S1. Crystallographic data

Zn_{0.994}Co_{0.006}	
Molecular formula	C ₁₆ H ₂₆ N ₄ O ₈ Zn
Molecule weight	467
Crystal system	Orthorhombic
Space group	<i>Pccn</i>
<i>a</i> , Å	15.2423
<i>b</i> , Å	9.3278
<i>c</i> , Å	13.0916
α , °	90
β , °	90
γ , °	90
<i>V</i> , Å ³	1864.33
<i>Z</i>	1

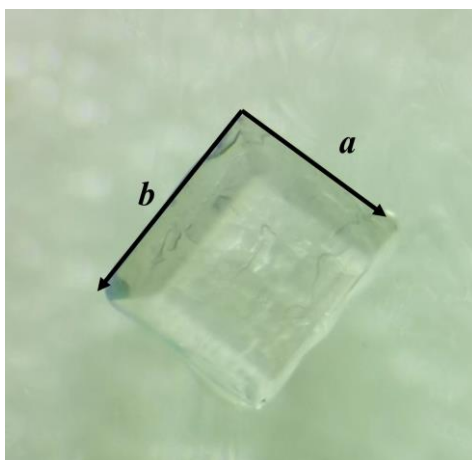


Fig.S1. (a) The result of face indexing showing on a physical crystal. The markings represent crystallographic *a*-axis and *b*-axis respectively.

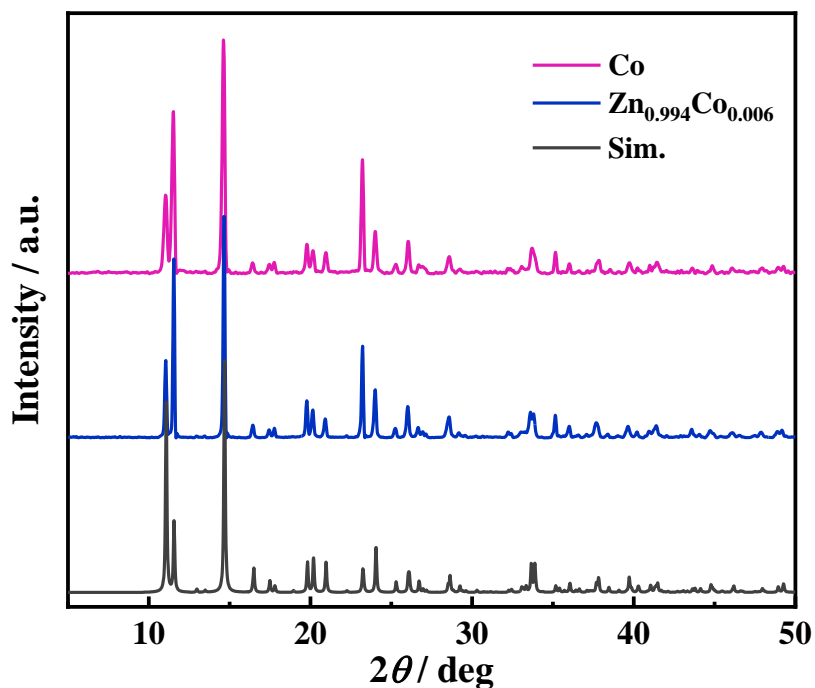


Fig.S2. Powder X-ray diffraction (PXRD) patterns of Co(H₂dota) (**Co**) and Zn_{0.994}Co_{0.006}(H₂dota) (**Zn_{0.994}Co_{0.006}**). The simulated pattern (**Sim.**) is also shown for comparison.

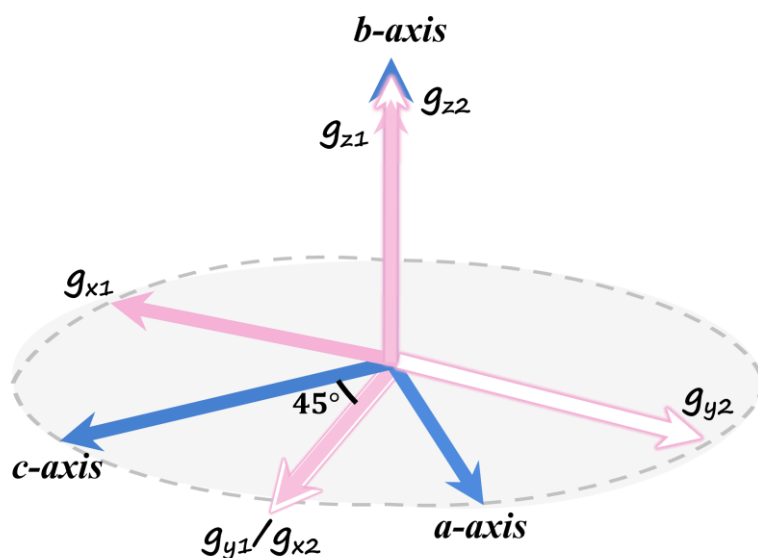


Fig.S3. Relative position between the crystal frame (*a*-axis, *b*-axis, *c*-axis) and tensor frames of two magnetically inequivalent Co(II) sites. The Euler transformations from the crystal frame to tensor frame of Co-1 and Co-2 are $\bar{R}_1(-90^\circ - 90^\circ - 45^\circ)$, $\bar{R}_2(-90^\circ - 90^\circ 45^\circ)$ respectively.

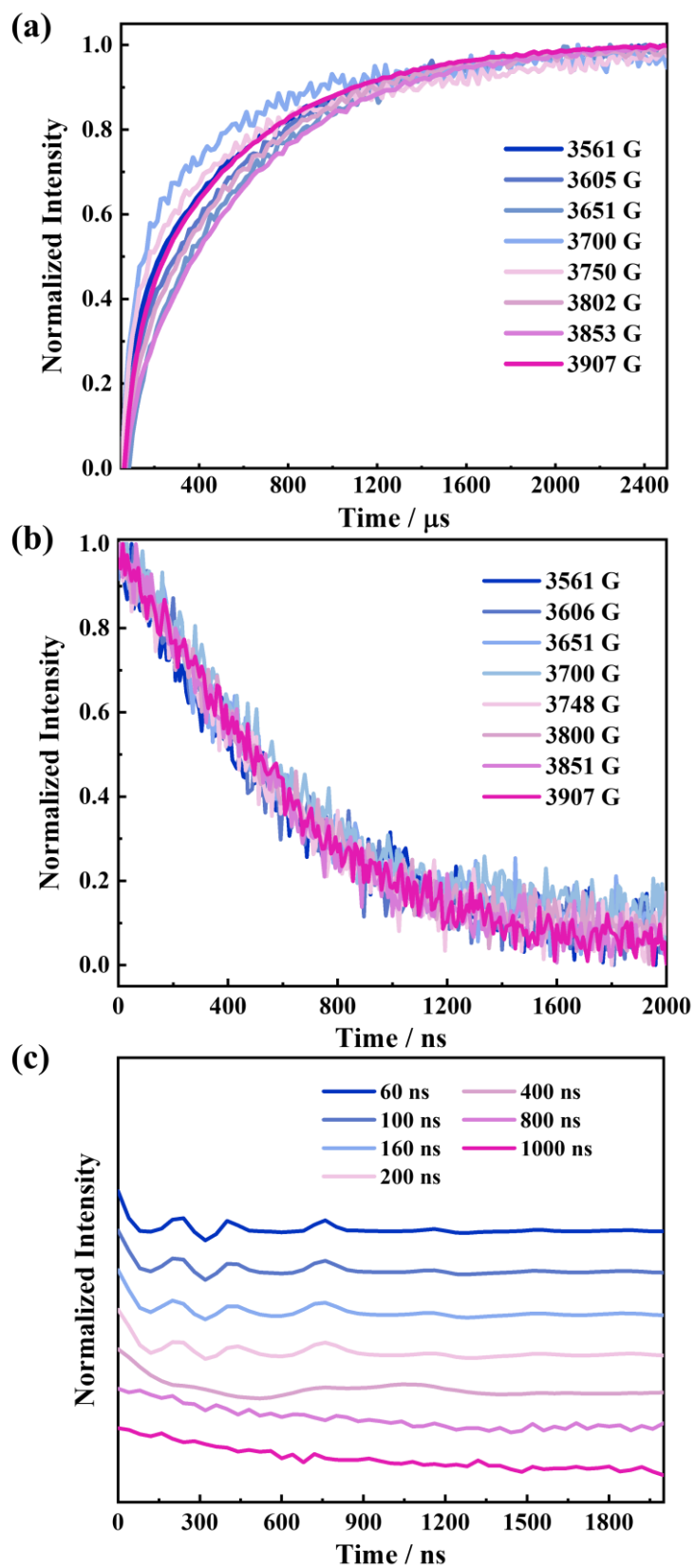


Fig.S4. T_1 (a) and T_m (b) curves at 5 K when $B_0 \parallel \mathbf{b}$. (c) T_m curves measured by different pulse lengths at 5 K by AWG and variation of ESEEM observed.

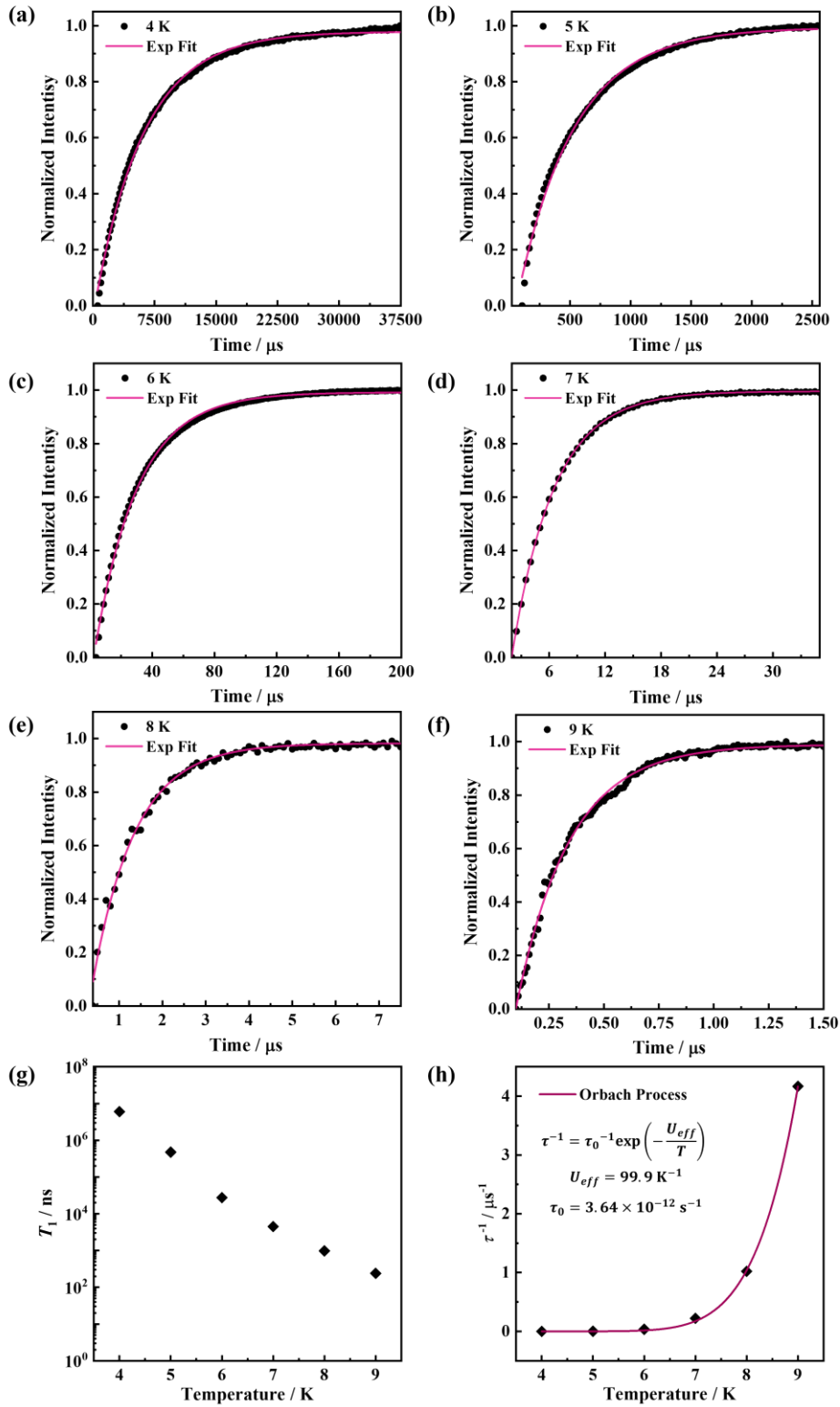


Fig.S5. (a)-(f) T_1 data (black point) measured at different temperatures at 3907 G and individual exponential fitting curves (wine line). (g) Temperature dependence of T_1 at 3907 G. (h) Fitting the spin relaxation mechanism.

Table S2. T_1 and T_m data at 5 K when $B_0 \parallel \mathbf{b}$.

B_0 / G	$T_1 / \mu\text{s}$	T_m / ns
3561	479.96	576.67
3606	498.94	563.50
3651	489.18	588.81
3700	444.07	600.69
3750	450.15	567.71
3802	490.17	606.86
3853	502.49	586.31
3907	475.27	664.97

Table S3. T_1 data between 4-9 K at 3907 G.

T / K	$T_1 / \mu\text{s}$
4	5995.39
5	475.27
6	27.45
7	4.51
8	0.98
9	0.24

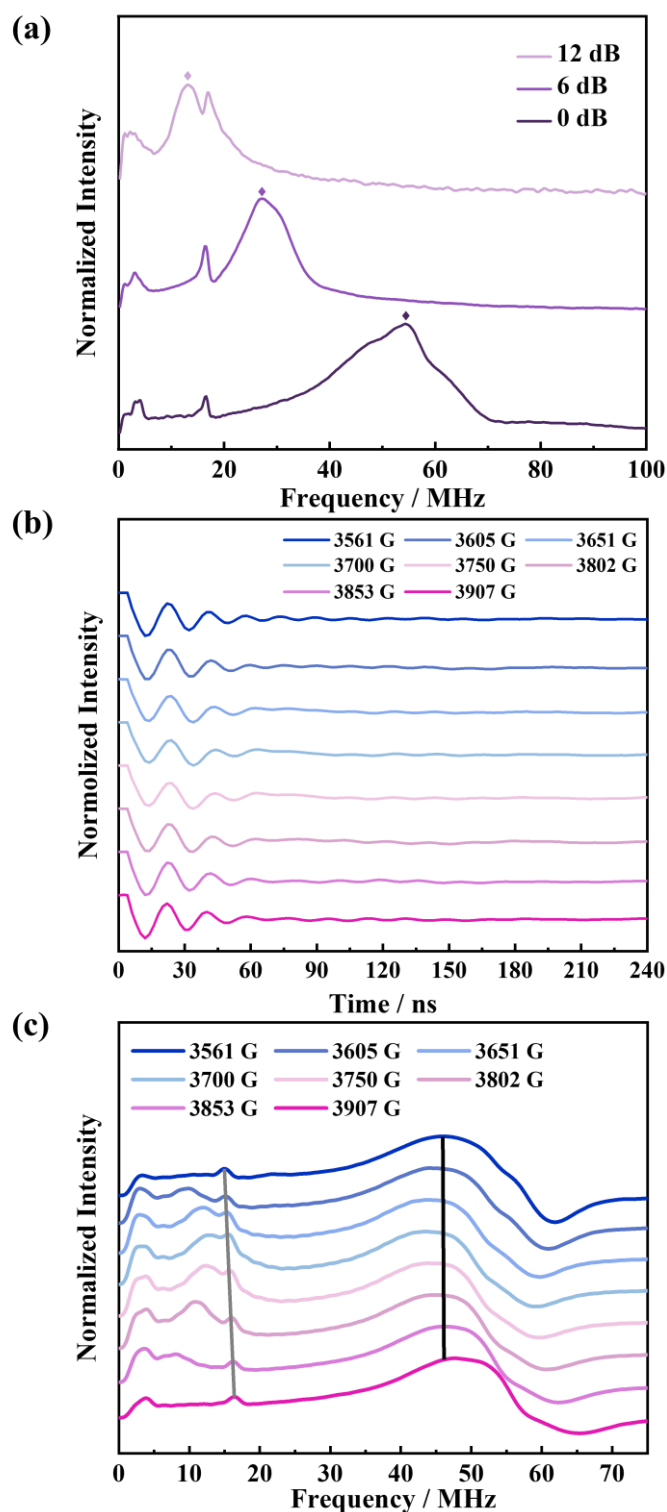


Fig.S6. (a) FFT of Rabi oscillations measured at 3907 G by a range of attenuation settings. (b) Rabi oscillations of the single crystal sample measured at different fields when $B_0 \parallel \mathbf{b}, B_1 \parallel \mathbf{a}$ at 5 K, 0 dB. (c) FFT of (b). Black and grey solid lines correspond to Rabi frequencies and ^1H Larmor frequencies respectively.

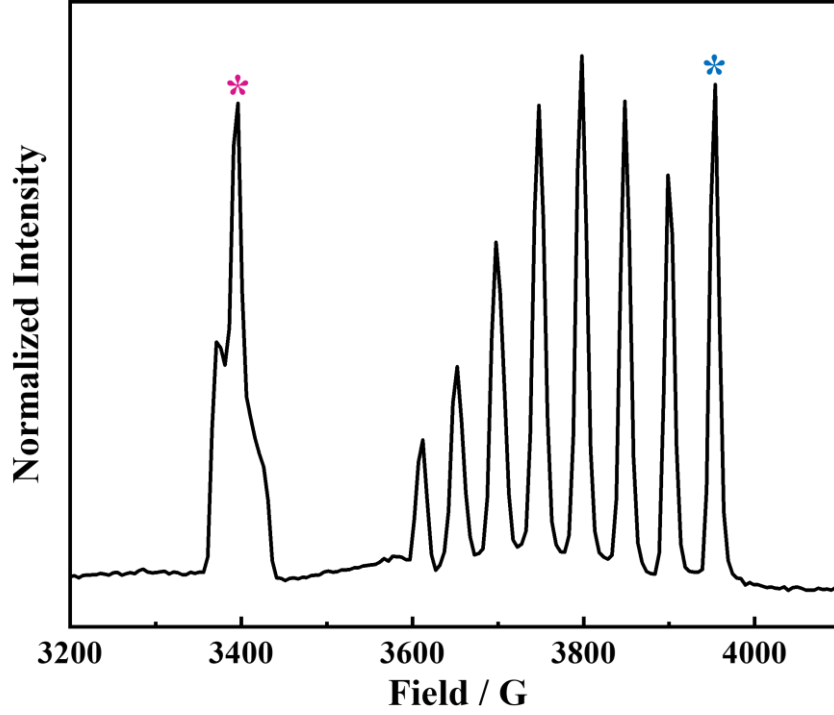


Fig.S7. EDFs of $\text{Zn}_{0.994}\text{Co}_{0.006}$ with internal standard TEMPO at 5 K, 0 dB when $B_0 \parallel \mathbf{b}$. The absolute values of experimental B_1 and g_{eff} are calibrated by the peak with wine mark. The Rabi oscillations of $\text{Zn}_{0.994}\text{Co}_{0.006}$ without specific description of B_0 field in Fig.S8-9 are measured on the transition with blue mark.

$$B_1 = \frac{\Omega_{\text{TEMPO}}}{\mu_B g_{\text{TEMPO}}} \quad (\text{Eq. S1 - 1})$$

$$g_{\text{eff}} = \frac{g_{\text{TEMPO}}}{\Omega_{\text{TEMPO}}} * \Omega_{\text{Sample}} \quad (\text{Eq. S1 - 2})$$

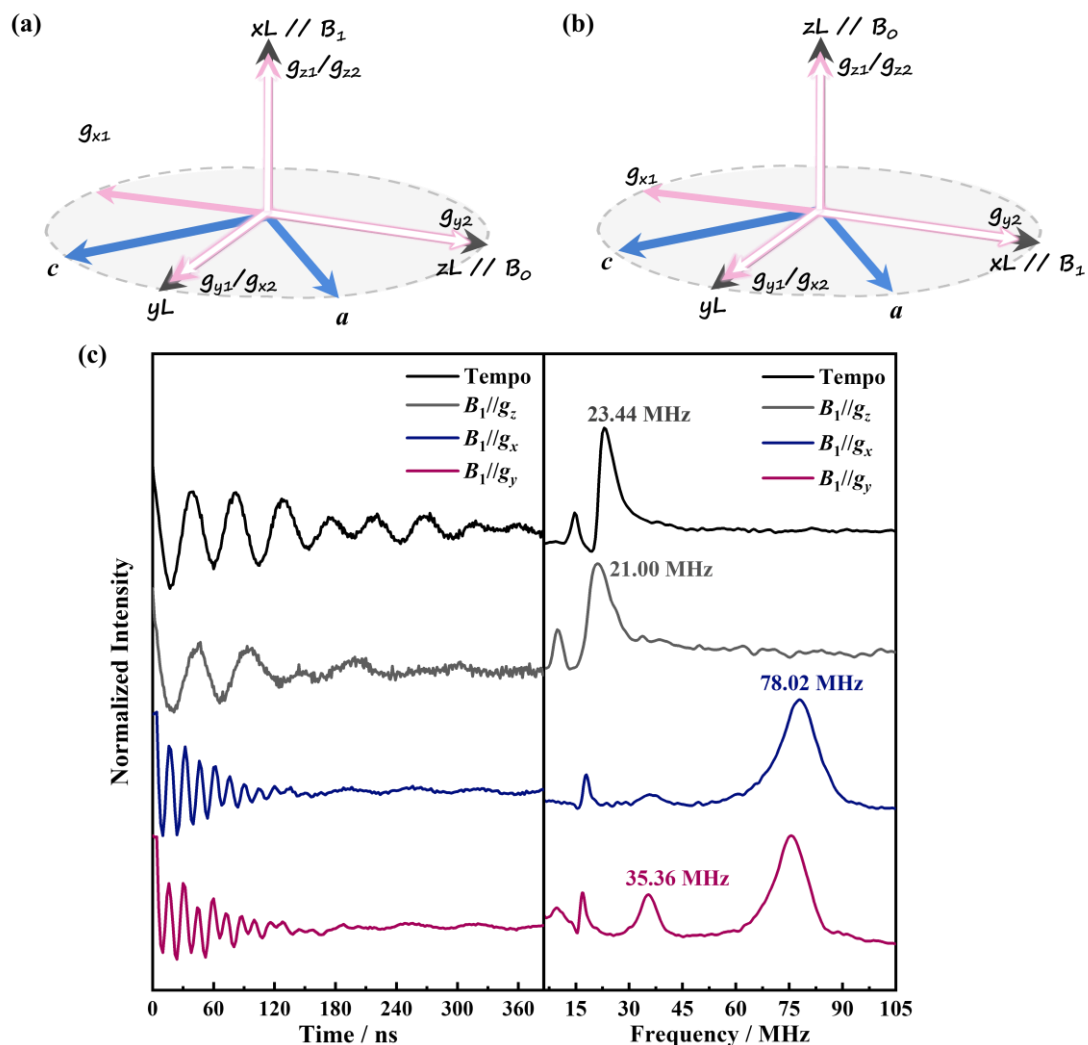


Fig.S8. Sketch of relative position between the lab frame and tensor frames in anisotropic Rabi oscillation experiments, depicting the case $B_1 \parallel g_z$ (a) and $B_1 \parallel g_{x,y}$ (b) respectively. The pink frame and white frame represent the tensor frames for Co-1 and Co-2 respectively. xL , yL , zL represent the lab frame (dark grey). zL is along the static magnetic field B_0 , xL is along microwave magnetic field B_1 . The blue frame represents crystal frame but b -axis is omitted. (c) Left: Rabi oscillations of internal standard TEMPO and $Zn_{0.994}Co_{0.006}$ crystal when $B_1 \parallel g_z$, g_x , g_y respectively. Right: FFT of Rabi oscillations shown on the left.

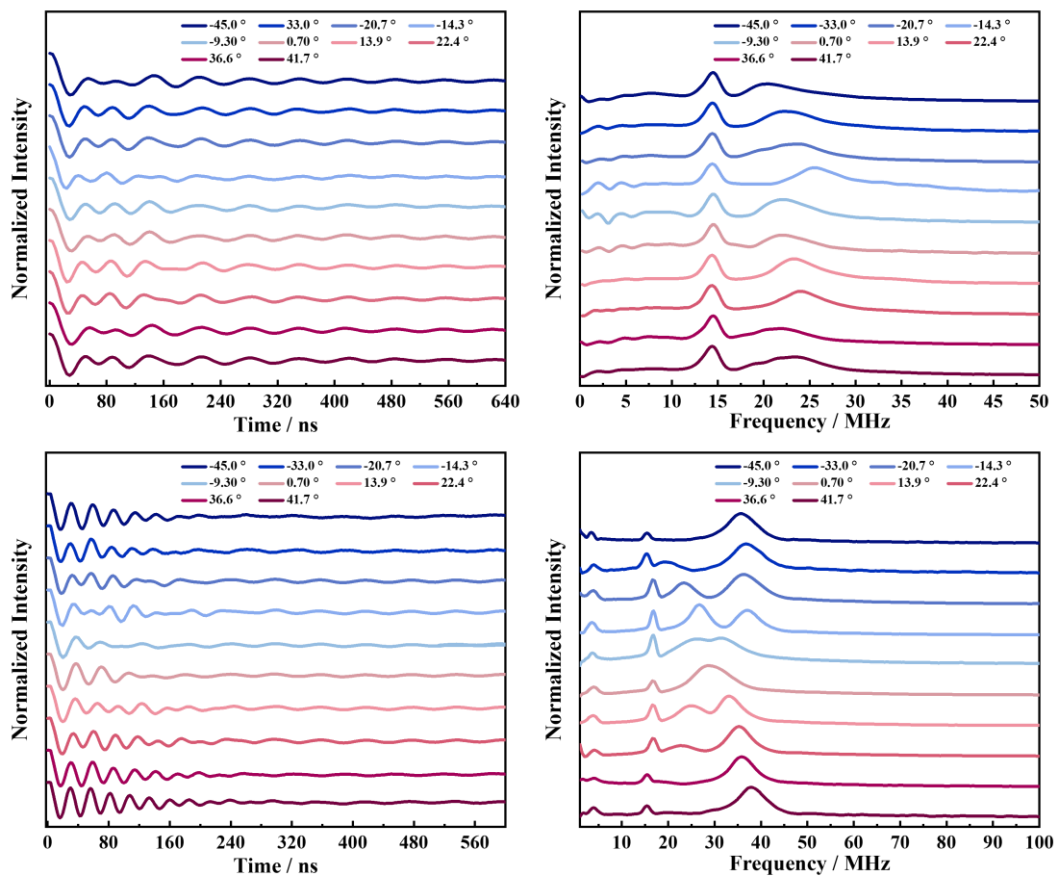


Fig.S9. Anisotropic Rabi oscillation experiments with internal standard. (a) Rabi oscillations of TEMPO measured with variable rotation angle α at 5 K, 0 dB. (b) FFT of (a). (c) Rabi oscillations of **Zn_{0.994}Co_{0.006}** measured with variable rotation angle α at 5 K, 6 dB. (d) FFT of (c).

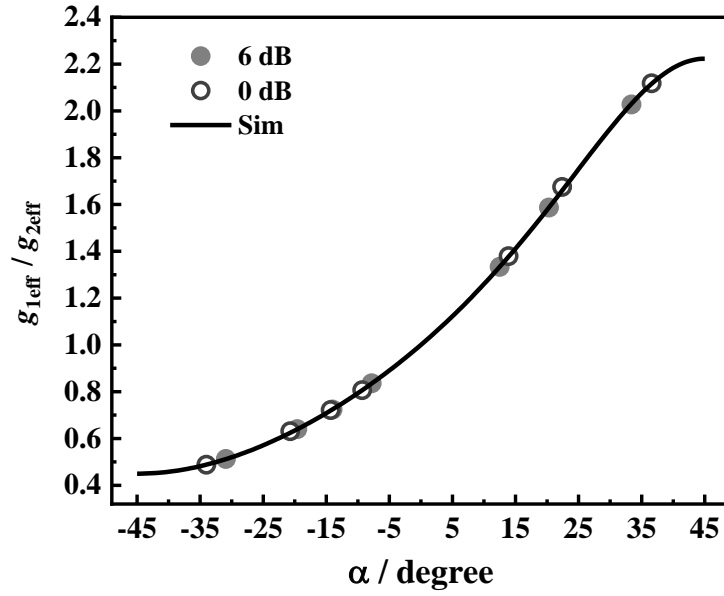


Fig.S10. Calibration of experimental rotation angle α . The black line is the calculated variation of g_{1eff}/g_{2eff} with α . Matching the ratio of two Rabi frequencies in Fig.4c (0 dB, open circle) and Fig.S9d (6 dB, grey circle) to calibrate experimental α .

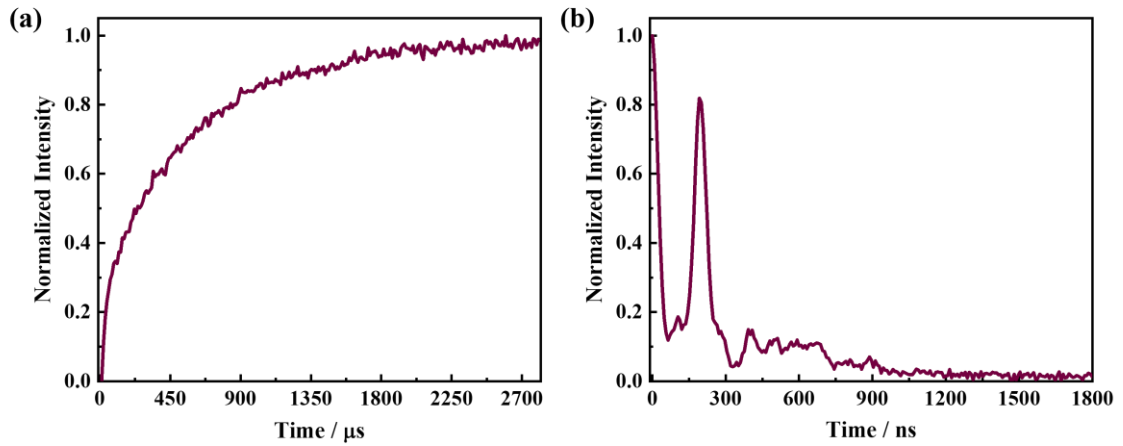


Fig.S11. T_1 (a) and T_m (b) curves at 5 K when B_0 is along g_y direction ($\pi/2 = 16$ ns, $\tau = 260$ ns). Modelling the curves with single exponential function as $T_1 = 457.67$ μ s and $T_M = 283$ ns.

SI 2 Theoretical analysis of anisotropic Rabi oscillation (I)

Considering a $S = \frac{1}{2}$ system with

$$\hat{H}_0 = \mu_B \vec{B} \vec{g} \hat{S}.$$

Based on the model shown in Fig.4a, i.e. $B_0 \parallel g_z$, g tensor should be expressed in lab frame as

$$\vec{g} = \bar{R}(\beta, 0, 0) \begin{pmatrix} g_x & 0 & 0 \\ 0 & g_y & 0 \\ 0 & 0 & g_z \end{pmatrix} \bar{R}^\dagger(\beta, 0, 0) = \begin{pmatrix} g_{xx} & g_{xy} & 0 \\ g_{yx} & g_{yy} & 0 \\ 0 & 0 & g_{zz} \end{pmatrix},$$

where $\bar{R}(\beta, 0, 0)$ and $\bar{R}^\dagger(\beta, 0, 0)$ represent the Euler rotation matrixes and

$$g_{zz} = g_z$$

$$g_{xx}(\beta) = g_x \cos \beta^2 + g_y \sin \beta^2 \quad (\text{Eq. S2 - 1})$$

$$g_{xy}(\beta) = (g_y - g_x) \cos \beta \sin \beta \quad (\text{Eq. S2 - 2})$$

The total Hamilton of the system is

$$\hat{H} = \hat{H}_0 + \hat{H}_1(t, \beta),$$

where

$$\hat{H}_0 = \mu_B B_0 g_z \hat{S}_z \quad (\omega_0 = \mu_B B_0 g_z),$$

$$\hat{H}_1(t, \beta) = \mu_B B_1 (\cos(\omega_{mw} t + \phi) \quad 0) \begin{pmatrix} g_{xx}(\beta) & g_{xy}(\beta) \\ g_{yx}(\beta) & g_{yy}(\beta) \end{pmatrix} \begin{pmatrix} \hat{S}_x \\ \hat{S}_y \end{pmatrix}.$$

We describe the system in a rotating frame with the microwave frequency ω_{mw} , the total Hamilton becomes

$$\hat{H}_{rot} = \hat{R}_z (\hat{H} - \omega_{mw} \hat{S}_z) \hat{R}_z^\dagger = \exp(i\omega_{mw} t \hat{S}_z) (\hat{H} - \omega_{mw} \hat{S}_z) \exp(-i\omega_{mw} t \hat{S}_z).$$

So

$$\hat{H}_{rot} = \frac{1}{2} \begin{pmatrix} \omega_0 - \omega_{mw} & \mu_B B_1 \cos(\omega t + \phi) (g_{xx}(\beta) - g_{xy}(\beta)i) e^{i\omega t} \\ \mu_B B_1 \cos(\omega t + \phi) (g_{xx}(\beta) + g_{xy}(\beta)i) e^{-i\omega t} & -(\omega_0 - \omega_{mw}) \end{pmatrix}.$$

Base on Euler's formula,

$$\hat{H}_{rot} = \frac{1}{2} \begin{pmatrix} \omega_0 - \omega_{mw} & \mu_B B_1 (g_{xx}(\beta) - g_{xy}(\beta)i) [e^{-i\phi} + e^{i(2\omega t + \phi)}] \\ \mu_B B_1 (g_{xx}(\beta) + g_{xy}(\beta)i) [e^{i\phi} + e^{-i(2\omega t + \phi)}] & -(\omega_0 - \omega_{mw}) \end{pmatrix}.$$

The terms $e^{\pm i(2\omega t + \phi)}$ can be neglected using the rotating wave approximation. Finally, in the resonance condition, $\omega_0 = \omega_{mw}$, and the total Hamilton can be expressed as

$$\hat{H}_{rot} = \frac{\mu_B B_1}{2} \begin{pmatrix} 0 & (g_{xx}(\beta) - g_{xy}(\beta)i)e^{-i\phi} \\ (g_{xx}(\beta) + g_{xy}(\beta)i)e^{i\phi} & 0 \end{pmatrix}.$$

For a general notation,

$$\hat{H}_{rot} = \mu_B B_1 [A(\beta, \phi) \hat{S}_x + B(\beta, \phi) \hat{S}_y], \quad (\text{Eq. S3 - 1})$$

where

$$A(\beta, \phi) = g_{xx}(\beta) \cos \phi - g_{xy}(\beta) \sin \phi, \quad (\text{Eq. S3 - 2})$$

$$B(\beta, \phi) = g_{xx}(\beta) \sin \phi + g_{xy}(\beta) \cos \phi. \quad (\text{Eq. S3 - 3})$$

Therefore, the rotation of spin in Bloch sphere will be determined by:

$$g_{eff}(\beta) = \sqrt{A^2 + B^2} = \sqrt{g_{xx}(\beta)^2 + g_{xy}(\beta)^2}, \quad (\text{Eq. S4 - 1})$$

$$\Phi(\beta, \phi) = \tan^{-1} \left(\frac{B}{A} \right). \quad (\text{Eq. S4 - 2})$$

$g_{eff}(\alpha)$ decides the nutation rate:

$$\Omega_{rabi}(\beta) = \mu_B B_1 \sqrt{g_{xx}(\beta)^2 + g_{xy}(\beta)^2}.$$

SI 3 Theoretical analysis of anisotropic Rabi oscillation (II)

Considering a $S = \frac{1}{2}$ system with

$$\hat{H}_0 = \mu_B \vec{B} \vec{g} \hat{S}.$$

Considering a model analogue to Fig.S8, i.e. B_1 coincides with a certain principal axis of the \vec{g} but B_0 does not. \vec{g} should be expressed in lab frame as

$$\vec{g} = \begin{pmatrix} g_{xx} & 0 & 0 \\ 0 & g_{yy} & g_{yz} \\ 0 & g_{zy} & g_{zz} \end{pmatrix}.$$

The static magnetic field Hamiltonian is

$$\hat{H}_0 = \mu_B \begin{pmatrix} 0 & 0 & B_0 \end{pmatrix} \begin{pmatrix} g_{xx} & 0 & 0 \\ 0 & g_{yy} & g_{yz} \\ 0 & g_{zy} & g_{zz} \end{pmatrix} \begin{pmatrix} \hat{S}_x \\ \hat{S}_y \\ \hat{S}_z \end{pmatrix} = \mu_B B_0 (g_{zy} \hat{S}_y + g_{zz} \hat{S}_z).$$

Diagonalize \hat{H}_0 and acquire the unitary transformation U and Larmor frequency as following

$$\hat{H}_0' = U \hat{H}_0 U^\dagger,$$

$$\omega_0 = \mu_B B_0 \sqrt{g_{zy}^2 + g_{zz}^2}.$$

Time dependent microwave Hamiltonian can be expressed as

$$\hat{H}_1(t) = \mu_B g_{xx} B_1 \cos(\omega t + \phi) \hat{S}_x.$$

Unitary transformation U will be used to rotate $\hat{H}_1(t)$ to eigen basis,

$$\hat{H}_1'(t) = U \hat{H}_1 U^\dagger.$$

The total Hamiltonian of the system is

$$\hat{H} = \hat{H}_0' + \hat{H}_1'(t).$$

We describe the system in a rotating frame with the microwave frequency ω_{mw} , the total Hamiltonian becomes

$$\hat{H}_{rot} = \hat{R}_z (\hat{H} - \omega_{mw} \hat{S}_z) \hat{R}_z^\dagger,$$

where

$$\hat{R}_z = \exp(i\omega_{mw} t \hat{S}_z).$$

So

$$\hat{H}_{rot} = \frac{1}{2} \begin{pmatrix} \omega_0 - \omega_{mw} & \mu_B B_1 g_{xx} \cos(\omega t + \phi) e^{i\omega t} \\ \mu_B B_1 g_{xx} \cos(\omega t + \phi) e^{-i\omega t} & -(\omega_0 - \omega_{mw}) \end{pmatrix}.$$

Base on Euler's formula,

$$\hat{H}_{rot} = \frac{1}{2} \begin{pmatrix} \omega_0 - \omega_{mw} & \mu_B B_1 g_{xx} [e^{-i\phi} + e^{i(2\omega t + \phi)}] \\ \mu_B B_1 g_{xx} [e^{i\phi} + e^{-i(2\omega t + \phi)}] & -(\omega_0 - \omega_{mw}) \end{pmatrix}.$$

The terms $e^{\pm i(2\omega t + \phi)}$ can be neglected using the rotating wave approximation. Finally, in the resonance condition, $\omega_0 = \omega_{mw}$, and the total Hamilton can be expressed as

$$\hat{H}_{rot} = \frac{1}{2} \begin{pmatrix} 0 & \mu_B B_1 g_{xx} e^{-i\phi} \\ \mu_B B_1 g_{xx} e^{i\phi} & 0 \end{pmatrix}.$$

Diagonalize \hat{H}_{rot} and Rabi frequency is therefore determined as

$$\Omega_{rabi} = \mu_B B_1 g_{xx}.$$

In our case shown in Fig.S8a, $g_{xx} = g_z$, so Rabi frequency is expressed as

$$\Omega_{Rabi} = g_z \mu_B B_1.$$